View metadata, citation and similar papers at core.ac.uk

brought to you by CORE

provided by Caltech Authors - Main

Journal of Applied Physics

Ab initio based investigation of thermal transport in superlattices using the Boltzmann equation: Assessing the role of phonon coherence

Cite as: J. Appl. Phys. **125**, 055107 (2019); https://doi.org/10.1063/1.5075481
Submitted: 22 October 2018 . Accepted: 15 January 2019 . Published Online: 05 February 2019

Erika Ye, and Austin J. Minnich

View Online Export Citation CrossMark

© 2019 Author(s).

Journal of Applied Physics ARTICLE scitation.org/journal/jap

Ab initio based investigation of thermal transport in superlattices using the Boltzmann equation: Assessing the role of phonon coherence

Cite as: J. Appl. Phys. **125**, 055107 (2019); doi: 10.1063/1.5075481
Submitted: 22 October 2018 · Accepted: 15 January 2019 ·
Published Online: 5 February 2019

View Online Export Citation CrossMark

Erika Ye and Austin J. Minnich

AFFILIATIONS

Division of Engineering and Applied Science, California Institute of Technology, Pasadena, California 91125-0002, USA

ABSTRACT

The role of the coherent interference of phonons on thermal transport in artificial materials such as superlattices is of intense interest. Recent experimental studies report a non-monotonic trend in thermal conductivity with interface density which is attributed to band-folding of thermal phonons. Various models have been proposed to interpret these measurements, but most make simplifying assumptions that make definitively attributing the trends to the coherent transport difficult. Here, we investigate thermal transport in superlattices in the incoherent limit using the Boltzmann equation with intrinsic phonon dispersions and lifetimes calculated from first-principles. We find that the Boltzmann equation is unable to predict the non-monotonic behavior of thermal conductivity versus superlattice period, supporting the interpretation of phonon interference in recent experiments.

Published under license by AIP Publishing. https://doi.org/10.1063/1.5075481

I. INTRODUCTION

Engineering the thermal transport properties of materials is an area of active research, particularly for thermoelectric materials.[1–4] Typical strategies to decrease thermal conductivity involve introducing microstructural features such as grain boundaries that lead to increased scattering and lower thermal conductivity. However, at length scales comparable to phonon wavelengths, the wave nature of phonons can have a significant impact. For example, the ultralow thermal conductivity of silicon nanowire cages is believed to be a result of localized phonon resonances.[5–7] Many works have reported the fabrication of acoustic metamaterials[8–10] and phononic crystals for vibrations with frequencies up to a few hundred GHz.[11–14] However, whether these effects are still relevant at THz frequencies despite atomic imperfections and anharmonic scattering, and thereby affect the transport of heat, remains a topic of debate.

Several experiments investigating the thermal conductivity of 1-D binary superlattices in the perpendicular direction report that the phonon coherence does play a role.[15–19] Most notable is the observation of a thermal conductivity minimum as superlattice period is varied.[15,16,20–22] This trend was predicted by Simkin and Mahan as an indicator of a transition between coherent and incoherent transport regimes.[23] They performed lattice dynamical calculations on a superlattice unit cell to obtain the folded band structure, and then used the new group velocities to calculate the superlattice thermal conductivity assuming a constant mean-free path. Subsequent work was reported by Chen,[24] who employed transfer matrices and ray tracing to find that the thermal conductance in the wave limit can be higher than in the particle limit. Yang and Chen expanded on the Simkin-Mahan model by introducing an imaginary component of the wave vector that varied with interface specularity and angle of incidence to account for diffuse scattering.[25] They found that diffuse scattering would suppress the minimum, consistent with the idea that only a fraction of the phonons are still specularly scattered. Their work assumed a constant mean free path.

However, phonons of different frequencies can have significantly different properties, and prior works have shown that neglecting these differences yields inaccurate results compared to *ab initio* predictions.[26,27] As a result, other works have employed atomistic computational techniques free of this assumption to examine phonon transport in superlattices.[18,19,28–35]. For example, computational

methods used include density functional theory (DFT) for short period superlattices[29,30] or molecular dynamics[28,32–37]. Atomistic Green's functions are another method, though including anharmonic interactions is challenging. These works all indicate that thermal conductivity increases as the superlattice layer thickness decreases, in agreement with the lattice-dynamical works. However, some predictions, such as how interface disorder affects the thermal conductivity, differ with each technique. Garg and Chen, using DFT, reported the observation of a thermal conductivity minimum even with disorder,[29] but the works based on molecular dynamics did not observe this minimum.[28,32,39] This discrepancy led to questions on the validity of the existing lattice dynamical models to explain experimental observations of the minimum, as samples are expected to exhibit at least somewhat diffuse interfacial scattering due to fabrication imperfections.

With these atomistic computational methods, phonons are treated as waves and thus it cannot be determined whether the thermal conductivity minimum can be explained in the particle limit simply by accounting for the spectral properties of phonons. So far, there are limited reports of calculating the thermal conductivity from the incoherent limit of particle transport based on the Boltzmann transport equation (BTE). Chen reported a methodology to compute the thermal conductivity of superlattices, but this work did not account for spectral phonon properties.[40] Recent works made other simplifying assumptions. For instance, several works have reported a modified Fourier's Law to approximately capture the size effects in the superlattice, but these works cannot explicitly account for modal transmission and reflection at an interface.[41–43] Hua and Minnich presented a method to solve the BTE in a 2-layer system using a cosine series expansion, making the computation efficient enough to eliminate the gray assumption.[44] However, their work must be adapted to describe periodic superlattices and include modal transmission and reflection at the interfaces.

Here, we report a method to solve the BTE and thereby compute the thermal conductivity of a 1-D periodic binary superlattice with *ab initio* inputs. We then use this method to examine how the thermal conductivity of the superlattice is affected by the superlattice period and the transmission properties of the interfaces. Our calculations indicate that the BTE is unable to predict a thermal conductivity minimum if transmission coefficients are independent of superlattice period, even when *ab initio* phonon properties are incorporated. Our result supports the interpretation of phonon coherence as the origin of the thermal conductivity minimum reported experimentally.

II. THEORY

We aim to calculate the thermal conductivity of a 1-dimensional binary superlattice (SL) with *ab initio* phonon properties and with specified modal transmission coefficients at the interface. In this section, we present the framework for solving the thermal conductivity of a system with a single interface, and then show how it can be generalized to handle multiple interfaces and periodic boundary conditions. We also discuss how partial transmission and partial scattering can be incorporated into interface boundary conditions.

In a SL, within each layer, phonons may scatter by anharmonic interactions, processes that are captured by the finite bulk lifetimes obtained from first-principles.[45] At each interface, phonons are transmitted with a probability specified by transmission coefficients and a specularity that varies with phonon wave vector. Hua *et al.* previously reported an efficient solution to the Boltzmann equation of a single slab for an isotropic solid.[44] In this work, we remove the isotropic approximation, enabling us to consider angle-dependent transmission coefficients. Furthermore, we demonstrate how this method can be generalized to handle multiple interfaces and implement periodic heat flux boundary conditions.

A. General solution

For simplicity, in this work, we will focus on the steady-state, 1-D Boltzmann Transport Equation (BTE) with no internal heat generation. In this case, the linearized BTE with the relaxation time approximation can be written as[44]

$$v_{gx,\lambda}\frac{\partial g_\lambda}{\partial x} = -\frac{g_\lambda - C_\lambda \Delta T}{\tau_\lambda}, \tag{1}$$

where x is the spatial coordinate in the cross-plane direction, $v_{gx,\lambda}$ is the group velocity in the x direction, C_λ is the modal heat capacity, τ_λ is the phonon lifetime, and g_λ is the local phonon energy distribution deviation, defined as

$$g_\lambda = \hbar\omega_\lambda[f_\lambda - f_{BE,\lambda}(T_0)]. \tag{2}$$

Here, f_λ is the unknown phonon distribution function for each mode, $f_{BE,\lambda}$ is the Bose-Einstein distribution, $\hbar$ is the reduced Planck's constant, ω_λ is the phonon frequency, and T_0 is a reference temperature. The subscript λ denotes the polarization and wave vector $\vec{k}$ of each mode in the Brillouin zone.

Equation (1) is a 1-D ordinary differential equation. The forward propagating and backward propagating solutions for g_λ, where $\hat{x} = x/L$ is the normalized distance, are respectively,

$$g_\lambda^+(\hat{x}) = P_\lambda e^{-\gamma_\lambda \hat{x}} + \int_0^{\hat{x}} \frac{C_\lambda \Delta T(\hat{x}')}{Kn_\lambda} e^{-\gamma_\lambda(\hat{x}-\hat{x}')}\, d\hat{x}' \text{ for } v_{gx,\lambda} > 0, \tag{3a}$$

$$g_\lambda^-(\hat{x}) = B_\lambda e^{\gamma_\lambda(1-\hat{x})} - \int_{\hat{x}}^1 \frac{C_\lambda \Delta T(\hat{x}')}{Kn_\lambda} e^{\gamma_\lambda(\hat{x}'-\hat{x})} d\hat{x}' \text{ for } v_{gx,\lambda} \le 0, \tag{3b}$$

where $\Delta T(\hat{x})$ is the local deviation in temperature from T_0, P_λ, and B_λ are coefficients defined by boundary conditions at the

Published under license by AIP Publishing.

edges of the slab, $\mathrm{Kn}_\lambda = v_{gx,\lambda}\tau_\lambda/\mathrm{L}$ is the modal Knudsen number, and $\gamma_\lambda = 1/\mathrm{Kn}_\lambda$. The modal deviational heat flux is

$$q_\lambda^\pm = g_\lambda^\pm v_{gx,\lambda} \tag{4}$$

and the thermal conductivity is

$$\kappa = \sum_\lambda \frac{q_\lambda^+ - q_\lambda^-}{(\Delta T_\mathrm{R} - \Delta T_\mathrm{L})\mathrm{L}}, \tag{5}$$

where ΔT_L and ΔT_R are the temperature offsets defined at the left and right edges of the slab.

The deviational phonon energy distribution is related to the deviational temperature profile $\Delta T(\hat{x})$ by conservation of energy

$$\sum_\lambda \left[\frac{g_\lambda(\hat{x})}{\tau_\lambda} - \frac{C_\lambda}{\tau_\lambda}\Delta T(\hat{x})\right] = 0. \tag{6}$$

Combining Eqs. (3) and (6), we obtain an integral equation for $\Delta T(\hat{x})$

$$\left(\sum_\lambda \frac{C_\lambda}{\tau_\lambda}\right)\Delta T(\hat{x}) = \sum_\lambda \frac{1}{\tau_\lambda}\left[P_\lambda e^{-\gamma_\lambda \hat{x}} + B_\lambda e^{-\gamma_\lambda(1-\hat{x})} + \int_0^1 \frac{C_\lambda \Delta T(\hat{x}')}{\mathrm{Kn}_\lambda} e^{-\gamma_\lambda|\hat{x}'-\hat{x}|} d\hat{x}'\right], \tag{7}$$

which is a Fredholm integral of the second kind, as it is of the form

$$\Delta T(\hat{x}) = f(\hat{x}) + \int_0^1 K(\hat{x}, \hat{x}')\Delta T(\hat{x}')\, d\hat{x}'. \tag{8}$$

A numerical solution to $\Delta T(\hat{x})$ can be found by expanding f and K as a cosine expansion with N terms. After some mathematical manipulation as detailed in Ref. 44, one can write $\Delta T(\hat{x})$ as a matrix equation

$$\Delta T(\hat{x}; \vec{P}, \vec{B}) = \mathbf{\Phi}(\hat{x})\left(\mathbf{I} - \frac{1}{2}\mathbf{K}\right)^{-1}\left(\mathbf{F}^1\vec{P} + \mathbf{F}^2\vec{B}\right). \tag{9}$$

Here, $\mathbf{\Phi}(\hat{x})$ is a matrix of the cosines used in the expansion. Values of the cosines with spatial frequencies $m\pi$, where m is an integer from 0 to N, evaluated at various $\hat{x}$ are along each column. The vectors $\vec{P}$ and $\vec{B}$ are defined by the boundary conditions and contain N_λ values, where N_λ is the total number of phonon modes. The $(\mathrm{N}+1)\times(\mathrm{N}+1)$ matrix $\mathbf{K}$ contains the cosine expansion coefficients of the kernel $K(\hat{x}, \hat{x}')$. The F matrices correspond to the cosine expansion coefficients for the inhomogeneous term $f(\hat{x})$ and are of dimension $(\mathrm{N}+1)\times \mathrm{N}_\lambda$. Explicit expressions for the matrix elements are given in Appendix A.

B. Solution for a binary superlattice

We consider a binary superlattice as shown in Fig. 1. For generality, we will denote the thicknesses of the two layers as L_1 and L_2, though in our calculations the two are the same. We will use the following notation: all material parameters will be written as vectors where each element is the value for a specific phonon mode. Material parameters for a specific mode will be referred to using superscripts (i, j, λ). Subscripts (α, β) will denote the layer. If subscripts are omitted, then the expression is valid for all layers generally. When the superscripts are omitted, we are referring to all phonon modes. Matrices will be bolded and vectors will have an arrow. For example, $\vec{C}_1$ refers to the modal heat capacities for all phonon modes in layer 1, and C_1^λ refers to the heat capacity of the phonon indexed by λ in layer 1. Multiplication of two vectors, such as $\vec{v}_{gx}\vec{C}$, corresponds to elemental multiplication. Multiplication of a matrix and a vector follows ordinary matrix algebra.

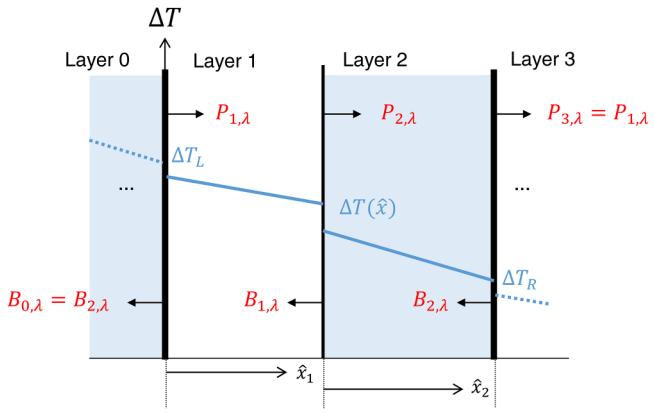

FIG. 1. Schematic of the binary 1-D superlattice model system consisting of a unit cell of two layers with periodic boundary conditions. $\Delta T(\hat{x})$ is the deviation of the local temperature with respect to the equilibrium temperature, and ΔT_L and ΔT_R are the temperatures specified at the left and right boundaries, respectively. $\hat{x}_\alpha$ is the spatial coordinate for layer α normalized by layer thickness L_α. The variables $P_{\alpha,\lambda}$ and $B_{\alpha,\lambda}$ are the coefficients of the inhomogeneous solution of the Boltzmann equation, which determine the heat flux propagating in the forward and backward direction. The λ subscript indexes phonon mode and the α is the numerical subscript indicating the layer.

1. Interface conditions

At the interfaces, both in the center of the domain and at the periodic boundary, phonons may be either transmitted or reflected. The interface conditions enforce heat flux conservation and are given by

$$\vec{q}_2^+ = \mathbf{T}_{12}\vec{q}_1^+ + \mathbf{R}_{21}\vec{q}_2^-, \tag{10a}$$

$$\vec{q}_1^- = \mathbf{R}_{12}\vec{q}_1^+ + \mathbf{T}_{21}\vec{q}_2^-. \tag{10b}$$

Here, $\mathbf{R}_{\alpha\beta}$ is a $(\mathrm{N}_{\lambda,\alpha}\times \mathrm{N}_{\lambda,\alpha})$ matrix specifying the reflection coefficients of phonons in layer α from layer β. $\mathbf{T}_{\alpha\beta}$ is a $(\mathrm{N}_{\lambda,\alpha}\times \mathrm{N}_{\lambda,\beta})$ matrix describing the transmission of phonons from layer α into layer β. We assume elastic transmission, and so we only define transmission between phonons of the

Published under license by AIP Publishing.

same frequency, ω. For each ω, the reflection and transmission matrices are subject to the following constraints of power conservation and time reversal symmetry, respectively,

$$\sum_j R_{12}^{ij} + T_{21}^{ij} = 1, \tag{11}$$

$$\sum_i R_{12}^{ij} + T_{12}^{ij} = 1, \tag{12}$$

$$\mathbf{R_{12}} = \mathbf{R_{12}}^{\mathrm{T}}, \tag{13}$$

$$\mathbf{T_{12}} = \mathbf{T_{21}}^{\mathrm{T}}, \tag{14}$$

and detailed balance

$$\sum_{\lambda\in\omega} \mathbf{T_{12}}\vec{q}_{0,1}^{+} = \sum_{\lambda\in\omega} \mathbf{T_{21}}\vec{q}_{0,2}^{-}, \tag{15}$$

where $q_0^\lambda = C^\lambda v_{gx}^\lambda T_0$ is the equilibrium heat flux for each phonon mode. These equations apply to all modes i and j of the same frequency ω, indicated by the notation $\lambda \in \omega$.

2. Partial specularity

Our modal approach allows us to account for reflection and transmission between an arbitrary set of phonons of the same frequency; therefore, we can also consider partially specular interfaces. For specular transmission, phonons must satisfy transverse momentum conservation in addition to energy conservation; for diffuse transmission, phonons only need to satisfy energy conservation. We neglect any anharmonic couplings across the interface. However, if the reflection or transmission is completely diffuse, the block matrix $ABCD$ becomes singular and one cannot solve for $\Delta T(\hat{x})$. To allow for partial specularity, we define separate sets of coefficients for the specular problem $(\vec{P}_s, \vec{B}_s)$ and the diffuse problem $(\vec{P}_d, \vec{B}_d)$. Diffuse coefficients $\vec{P}_d$ and $\vec{B}_d$ each only contain N_ω unknown variables, where $N_\omega < N_\lambda$ is the number of frequency bins.

We define the partial specularity for each phonon frequency p^ω with respect to the deviational distribution of the phonon mode as

$$p^\omega = \frac{\sum_{\lambda\in\omega} P_s^\lambda}{\sum_{\lambda\in\omega} P_s^\lambda + P_d^\omega}. \tag{16}$$

A similar expression can be defined for backwards propagating modes.

Using these specularity conditions, in addition to the conservation of heat flux at the interface as described in Sec. II B 1, we can solve for the specular and diffuse coefficients. Details of the extended block matrix system of equations to account for specularity are included in Appendix B 2.

3. Periodic boundary conditions

To consider binary superlattices of infinite thickness, we must apply periodic boundary conditions at the two ends of a single unit cell. As described in Refs. 46 and 47, the deviational phonon energy distribution at the boundaries is defined to be periodic, meaning that the coefficients $\vec{P}$ and $\vec{B}$ are also periodic. However, the temperature profile in each unit cell is not periodic. As a result, the black-body phonon radiation contribution $C^\lambda v_{gx}^\lambda T_0$ is also different for each unit cell, and the difference must be included at the boundaries.

More precisely, let $\Delta T_0 = \Delta T_L - \Delta T_R$ denote the temperature difference between two adjacent unit cells, or equivalently, the temperature difference imposed at the ends of the unit cell. Then, the deviational heat fluxes at the interface between layers 2 and 3 are related to the deviational heat fluxes at the interface between layers 0 and 1 by

$$\vec{q}_3^{+}(\hat{x}_3 = 0) = \vec{q}_1^{+}(\hat{x}_1 = 0) + (\vec{C}_1\vec{v}_{gx,1})\Delta T_0, \tag{17a}$$

$$\vec{q}_2^{-}(\hat{x}_2 = 1) = \vec{q}_0^{-}(\hat{x}_0 = 1) + (\vec{C}_2\vec{v}_{gx,2})\Delta T_0. \tag{17b}$$

Combining the above with Eq. (10), and rewriting all the components in terms of values in layers 1 and 2, we obtain the boundary conditions

$$\begin{aligned}\vec{q}_1^{+}(x_1 = 0) + (\vec{C}_1\vec{v}_{gx,1})\Delta T_0 &= \mathbf{T_{21}}\vec{q}_2^{+}(x_2 = L_2)\\ &+ \mathbf{R_{12}}\left[\vec{q}_1^{-}(x_1 = 0) + (\vec{C}_1\vec{v}_{gx,1})\Delta T_0\right],\end{aligned} \tag{18a}$$

$$\begin{aligned}\vec{q}_2^{-}(x_2 = 0) &= \mathbf{R_{21}}\vec{q}_2^{+}(x_2 = L_2)\\ &+ \mathbf{T_{12}}\left[\vec{q}_1^{-}(x_1 = 0) + (\vec{C}_1\vec{v}_{gx,1})\Delta T_0\right].\end{aligned} \tag{18b}$$

C. Matrix formulation

To explicitly show the role of the coefficients $\vec{P}$, $\vec{B}$ at the interface between layers α and $\alpha+1$, we write the boundary conditions as a matrix equation (in block matrix form)

$$\begin{bmatrix} A & B \\ C & D \end{bmatrix}\begin{bmatrix} B_\alpha \\ P_{\alpha+1} \end{bmatrix} = \begin{bmatrix} E & 0 \\ F & 0 \end{bmatrix}\begin{bmatrix} B_{\alpha+1} \\ P_{\alpha+2} \end{bmatrix} + \begin{bmatrix} 0 & G \\ 0 & H \end{bmatrix}\begin{bmatrix} B_{\alpha-1} \\ P_\alpha \end{bmatrix}. \tag{19}$$

The two rows of the matrix correspond to the boundary conditions given by Eq. (10). A schematic showing the organization of the equations, as well as explicit expressions for blocks A through H, are in Appendix B 1. The unknown coefficients $(\vec{B}_\alpha, \vec{P}_{\alpha+1})$ are obtained by matrix inversion.

For a binary superlattice, there are two interfaces: one in the middle (between layers 1 and 2) with boundary conditions described by Eq. (10), and one at which the periodic boundary condition is applied (between layers 0 and 1), as given by Eq. (18). These two boundary conditions provide a system of

Published under license by AIP Publishing.

two equations with two unknown vectors

$$\begin{bmatrix} A & B \\ C & D \end{bmatrix}_{12} \begin{bmatrix} B_1 \\ P_2 \end{bmatrix} = \begin{bmatrix} E & G \\ F & H \end{bmatrix}_{12} \begin{bmatrix} B_2 \\ P_1 \end{bmatrix}, \tag{20a}$$

$$\begin{bmatrix} A & B \\ C & D \end{bmatrix}_{01} \begin{bmatrix} B_2 \\ P_1 \end{bmatrix} = \begin{bmatrix} E & G \\ F & H \end{bmatrix}_{01} \begin{bmatrix} B_1 \\ P_2 \end{bmatrix}. \tag{20b}$$

After solving for the coefficients B_1, P_2, B_2, and P_1, the thermal conductivity can be calculated by inserting them into Eqs. (3a) and (3b), and then using Eqs. (4) and (5). To find the temperature profile across one unit cell of the superlattice, the coefficients are inserted into Eq. (9).

The procedure to obtain the coefficients requires a matrix inversion to be performed. The size of matrix ABCD depends on the number of phonon modes in the bulk materials, so the computational cost increases as the number of k-points increases. To reduce the cost of the calculation, we use symmetry to consolidate degenerate phonon modes. First, we only consider the irreducible wedge of the Brillouin zone. Then, we account for rotational symmetry about the x-axis by grouping terms with wavevectors $(k_x, k_y, k_z) = (k_x, k_z, k_y)$. We also do not distinguish between otherwise equivalent modes by polarization. Modes are considered to be degenerate if the modal energies are within $v_{gx}\Delta k$ of each other, where Δk is the difference in k_x for adjacent k-points in the Brillouin zone mesh. This consolidation is accounted for in the weighting used when summing over all modes in the Brillouin zone.

D. Summary of calculation

In summary, the steps for solving the thermal conductivity and temperature profile for a binary superlattice with periodic boundary conditions are as follows. First, one uses the equations given in Appendix A to obtain the matrices in Eq. (9). Then, one builds the block matrix system of equations [Eq. (19)], describing the boundary conditions at the interface within the unit cell [Eq. (10)] and the interface between two unit cells [Eq. (18)]. With these two matrix equations, we then solve for the unknown coefficients P_1^λ, B_1^λ, P_2^λ, and B_2^λ. Using these coefficients, we can obtain $g^\lambda(x)$ and then use Eqs. (4) and (5) to obtain the thermal conductivity.

III. RESULTS

In this section, we present our calculations of the thermal conductivity of binary 1D superlattices with periodic boundary conditions. We define the superlattice to have layers of equal thickness L. To simplify the calculation, we assume that both constituent materials are silicon, giving a Si/Si superlattice; this is a reasonable approximation when the lattice spacing and dispersion of the two materials in the SL are similar. Making this approximation also simplifies the definition of the transmission and specularity at the interface, allowing us to investigate how these interface parameters affect the superlattice thermal conductivity. As we are working in the particle limit, these interface parameters are independent of superlattice period.

The full *ab initio* phonon dispersions and lifetimes for crystalline Si are obtained using density functional theory courtesy of Dr. Lucas Lindsay.[45] The data contain 2048 data points per phonon branch in the irreducible Brillouin zone. The dispersion relation can be found in the appendix of Ref. 45. In our thermal conductivity calculations, we assume that the superlattices are oriented in the [100] direction.

A. Uniform transmission coefficients

We first consider the cases for which specular transmission is unity for all modes (in accordance with the acoustic mismatch model, AMM), and for which diffuse transmission is 0.5 for all modes (in accordance with the diffuse mismatch model, DMM). The test cases of purely specular transmission ($p^\omega = 1$) and purely diffuse transmission ($p^\omega = 0$) provide evidence that the calculation is working properly. First, if the interfaces transmit phonons perfectly specularly the interfaces pose no resistance to heat flow and the thermal conductivity should be independent of SL period. On the other hand, if the interfaces are perfectly diffuse, the thermal conductivity decreases with decreasing period due to interface scattering, consistent with the well-known classical size effects.[48] These two results are indeed observed in Fig. 2(a). Clearly, neither of these cases exhibit a non-monotonic trend of thermal conductivity with superlattice layer thickness L.

We next investigate the behavior with partial specularity. For the first partially specular case, we use Ziman's definition of specularity,[49] obtaining

$$p^\omega = \sum_{\lambda \in \omega} \exp\left[-4\eta^2 (k_x^\lambda)^2\right], \tag{21}$$

where η is the interface roughness, chosen to be 0.8 Å so that the thermally occupied modes exhibit a broad range of specularities. In this case, we find that κ decreases with L similar to the purely diffuse case but has a higher overall thermal conductivity and decreases more slowly. The higher thermal conductivity is due the fact that some phonons still transmit specularly, and the slower decrease arises from a lower effective interface resistance.

Recently, it was suggested that by defining the specularity in relation to an interface density of states, the phonon transmission profile through the interface can be more accurately predicted.[50] This choice of specularity would still exhibit the same thermal conductivity trend as one decreases superlattice layer thickness. As L is decreased, phonons with non-unity transmission contribute less to thermal conductivity while phonons with near-unity transmission dominate the thermal conductivity. Since the interface density of states is independent of L in the present formalism, there is no mechanism by which the thermal conductivity could increase at smaller L.

B. Non-uniform transmission coefficients

In this section, we assume specular but non-unity transmission coefficients that vary with angle of incidence and

Published under license by AIP Publishing.

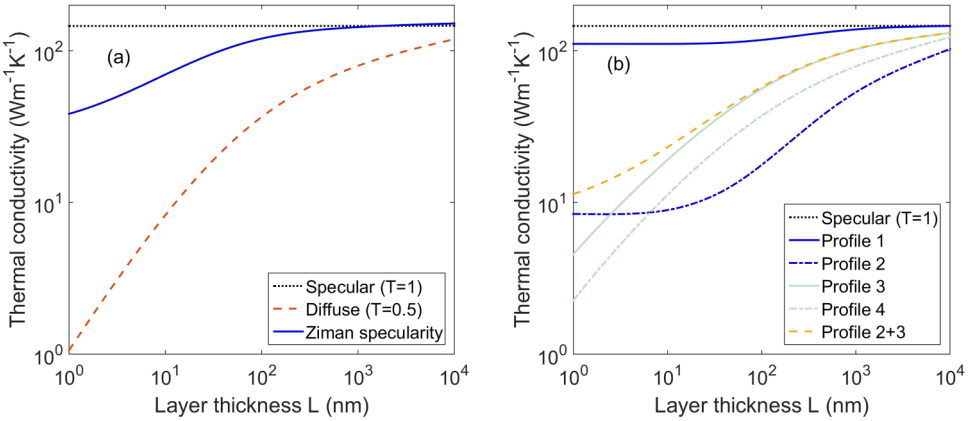

FIG. 2. (a) Thermal conductivity versus layer thickness L with different specularity parameters and uniform transmission. We consider specular transmission with unity transmission (dotted black), diffuse transmission with 50% transmission, in accordance with DMM (dot-dash red), and partially specular transmission with Ziman specularity assuming a roughness 0.8 Å (solid blue). For partially specular transmission, considering transmission with and without mode conversion yielded no discernible differences. (b) Thermal conductivity versus layer thickness for non-uniform transmission, assuming unity specularity. We consider 5 transmission profiles: **1.** (solid blue) a low pass frequency filter $T^{LP}(\omega; 0.3)$, **2.** (dot-dash blue) a high pass frequency filter $T^{HP}(\omega; 0.6)$, **3.** (solid light gray) a filter that preferentially transmits normally incident modes $T^{\perp}(k; 1)$, **4.** (dot-dash light gray) a filter that preferentially transmits angled-incidence modes $T^{\parallel}(k; 1)$, and **5.** (dashed yellow) a combination of profiles 2 and 3. Phonons with $\omega > 0.6\,\omega_{max}$ have unity transmission and phonons with $\omega < 0.6\,\omega_{max}$ are filtered by incident angle according to $T^{\perp}(k; 1)$. For reference, the bulk conductivity (equivalent to an interface with unity transmission and specularity) is shown in the dotted black line.

phonon frequency. In particular, we consider frequency filters, which emulate a mismatch between phonon density of states; and angle-dependent filters which emulate an impedance mismatch.

To capture these effects in our transmission and reflection matrices, we consider the following specular transmission matrices,

$$\mathrm{T}^{\mathrm{LP}}(\omega; a) = \Theta(\omega - a\omega_{max}), \tag{22a}$$

$$\mathrm{T}^{\perp}(k; b) = 1 - b(1 - |k_x|/|k|), \tag{22b}$$

$$\mathrm{T}^{\mathrm{HP}}(\omega; a) = 1 - \Theta(\omega - a\omega_{max}), \tag{23a}$$

$$\mathrm{T}^{\parallel}(k; b) = b(1 - |k_x|/|k|), \tag{23b}$$

where Θ is the Heaviside step function and a and b are constant parameters between 0 and 1 specified in the caption of Fig. 2. The reflection and transmission profiles given by Eq. (22) physically motivated, as the frequency filter [Eq. (22a)] is a low-pass (LP) filter while the wave-vector filter [Eq. (22b)] preferentially transmits phonons at normal incidence, in agreement with intuitive expectations of wave reflection and transmission. The second set of equations [Eq. (23)] are less physically motivated as the frequency filter is a high-pass (HP) and the wave-vector filter preferentially transmits phonons at shallow incident angles.

The thermal conductivity versus layer thickness for these cases is shown in Fig. 2(b). In the case of the frequency filters, as L decreases, the thermal conductivity first decreases but then reaches a plateau. This plateau corresponds to the contribution to thermal conductivity from phonons that propagate without reflection. The low-pass filter results in a plateau at a higher thermal conductivity than the high-pass filter results since low frequency phonons contribute more to thermal conductivity than the high frequency optical modes. In the case of the incident angle filters, as L decreases, the thermal conductivity continues to decrease, as only normally incident phonon modes (if $\mathrm{T}^{\perp}$) or phonons parallel to the interface (if $\mathrm{T}^{\parallel}$) are able to propagate without reflection. In all cases, the thermal conductivity does not exhibit a minimum as a function of L.

Though we only showed a few sample transmission and reflection coefficient choices, more general transmission coefficients can be obtained using superpositions of the filters. For example, the yellow curve in Fig. 2(b) corresponds to the thermal conductivity for a transmission profile that follows $\mathrm{T}^{\perp}(k; 1)$ for phonon frequencies below 0.3 ω_{max} and otherwise has unity transmission. The resulting thermal conductivity also does not exhibit a minimum. In general, one can build a variety of other transmission profiles of various shapes using the phonon filters given in Eqs. (22) and (23). However, since the thermal conductivity always is non-increasing with decreasing L, regardless of the phonon filter, we have not identified a transmission profile that will generate a non-monotonic thermal conductivity trend.

Our calculations therefore suggest that regardless of the dependence of the transmission coefficients on phonon frequency or incident angle, and regardless of specularity, the thermal conductivity is always non-increasing with decreasing SL period in the incoherent limit. Frequency filters effectively reduce the bulk thermal conductivity. Non-unity transmission matrices are equivalent to thermal resistors at

Published under license by AIP Publishing.

the interfaces and lead to reductions in the thermal conductivity with decreasing L.

We can also include the possibility of partially specular transmission using a similar analysis. As L decreases, the thermal conductivity will initially decrease as the phonons reflect from the interface more frequently. At some value of L, phonons with specular and near-unity transmission coefficients dominate the thermal conductivity and the thermal conductivity becomes independent of L. Therefore, in the particle picture, there is no obvious physical mechanism for the thermal conductivity to increase at smaller L.

C. Temperature dependence of thermal conductivity

Prior works have used the temperature dependence of the thermal conductivity to assess the role of phonon coherence on thermal conductivity. In Fig. 3, we present calculations of the thermal conductivity versus temperature for uniform transmission and non-uniform transmission coefficients for various specularities and layer thicknesses, as presented earlier.

We find that the thermal conductivity versus temperature trend qualitatively varies depending on the particular transmission coefficient profile and superlattice geometry. As expected, systems with unity transmission exhibit higher thermal conductivities at lower temperatures due to the longer phonon lifetimes. In contrast, systems with non-unity transmission may exhibit lower thermal conductivities at lower temperatures, depending on the transmission profile. In particular, reduction of thermal conductivity can occur when low-energy phonons have low probabilities of transmission at the interface (e.g. all phonons in the case of Interface 2, and the angled phonons in the case of Interface 4, as shown in Fig. 3). Therefore, while measuring thermal conductivity with respect to ambient temperature can provide some insight into the transmissivity of the phonons at each interface, making definitive conclusions on the role of phonon coherence in the thermal transport is challenging.

IV. CONCLUSION

In summary, we have reported a numerical method to solve the Boltzmann equation with *ab initio* inputs for 1-D superlattices with modal transmission coefficients. Applying this method to the thermal transport in superlattices, we find that the BTE is unable to predict the existence of a thermal conductivity minimum versus SL period, even with *ab initio* phonon properties and qualitatively different choices of transmission coefficients. Therefore, our study supports the interpretation that phonon coherence plays a role of thermal transport in recent experimental studies of binary superlattices.

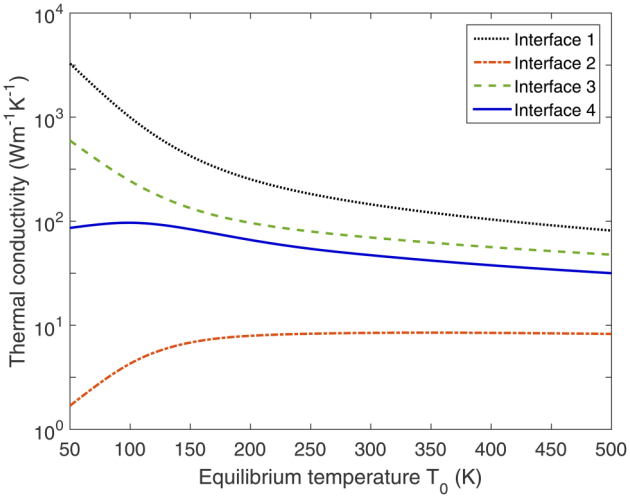

FIG. 3. Thermal conductivity versus temperature for several different superlattices. We consider the following interfaces: **1.** (dotted black) unity specularity with unity transmission, **2.** (dot-dash red) diffuse transmission coefficients with a value of 0.5, **3.** (dashed green) Ziman specularity with roughness of 0.8 Å, **4.** (solid blue) angle-dependent reflectivity ($b = 0.05$) with unity specularity. The layer thickness L is 10 nm.

APPENDIX A: COEFFICIENTS FOR COSINE EXPANSION

This appendix contains expressions for the elements $F^1_{m,\lambda}$, $F^2_{m,\lambda}$, and $K_{m,n}$ for the matrices F^1, F^2, and K in Eq. (9). In all of the following equations, the normalization factor is $M = 2\sum_k C_k/\tau_k$. Also, recall that $\hat{x}$ corresponds to the distance normalized by the thickness of the layer, L. These coefficients are generalized versions of those given in the Appendix of Ref. 44.

The kernel $K(x, x')$ is

$$K(\hat{x}, \hat{x}') = \frac{1}{M}\sum_{\lambda}\frac{C_\lambda}{Kn_\lambda\tau_\lambda}e^{-\gamma_\lambda|\hat{x}-\hat{x}'|}. \tag{A1}$$

The coefficients for the cosine expansion are

$$k_{mn} = \frac{c}{M}\int_0^1\int_0^1 K(\hat{x}, \hat{x}')\cos(m\pi\hat{x})\cos(n\pi\hat{x}')\,d\hat{x}\,d\hat{x}' = \begin{cases} \frac{c}{M}\sum_\lambda \frac{C_\lambda}{Kn_\lambda\tau_\lambda}\left(\frac{\{[(-1)^m+(-1)^n]e^{-\gamma_\lambda}+[-1-(-1)^{m+n}]\}\gamma_k^2}{(\gamma_\lambda^2+m^2\pi^2)(\gamma_\lambda^2+n^2\pi^2)}\right) & \text{if } m \neq n, \\ \frac{c}{M}\sum_\lambda \frac{C_\lambda}{Kn_\lambda\tau_\lambda}\left(\frac{e^{-\gamma_\lambda}[2(-1)^m\gamma_\lambda^2]+\gamma_\lambda[(\gamma_\lambda-2)\gamma_\lambda+m^2\pi^2]}{(\gamma_\lambda^2+m^2\pi^2)^2}\right) & \text{if } m = n \neq 0, \\ \frac{c}{M}\sum_\lambda \frac{C_\lambda}{Kn_\lambda\tau_\lambda}\left[\frac{2(-1+e^{-\gamma_\lambda}+\gamma_\lambda)}{\gamma_\lambda^2}\right] & \text{if } m = n = 0, \end{cases} \tag{A2}$$

Published under license by AIP Publishing.

where $c = 1$ if $m = n = 0$, $c = 2$ if either $m = 0$ or $n = 0$, or $c = 4$ if both $m, n \neq 0$.

The inhomogeneous term is $f(\hat{x}) = f_\lambda^1(\hat{x})P_\lambda + f_\lambda^2(\hat{x})B_\lambda$, where

$$f_\lambda^1(\hat{x}) = \frac{1}{M}\frac{1}{\tau_\lambda}e^{-\gamma_\lambda \hat{x}}, \tag{A3}$$

$$f_\lambda^2(\hat{x}) = \frac{1}{M}\frac{1}{\tau_\lambda}e^{-\gamma_\lambda(1-\hat{x})}. \tag{A4}$$

The cosine expansion coefficients $f_{m,\lambda}^i = c\int_0^1 f(\hat{x})\cos(m\pi\hat{x})\,d\hat{x}$ are

$$f_{m,\lambda}^1 = \frac{c}{M}\frac{1}{\tau_\lambda}\left(\frac{[1-(-1)^m e^{-\gamma_\lambda}]}{\gamma_\lambda(1+m^2\pi^2/\gamma_\lambda^2)}\right), \tag{A5}$$

$$f_{m,\lambda}^2 = \frac{c}{M}\frac{1}{\tau_\lambda}\left(\frac{[(-1)^m - e^{-\gamma_\lambda}]}{\gamma_\lambda(1+m^2\pi^2/\gamma_\lambda^2)}\right), \tag{A6}$$

where $c = 1$ if $m = 0$ and $c = 2$ otherwise.

APPENDIX B: BLOCK MATRIX NOTATION

1. Specular transmission

At the interface, to satisfy heat flux conservation, the following constraints must be satisfied

$$\vec{q}_2^{+}(x_2 = 0) = \mathbf{T_{12}}\vec{q}_1^{+}(x_1 = L_1) + \mathbf{R_{21}}\vec{q}_2^{-}(x_2 = 0), \tag{B1a}$$

$$\vec{q}_1^{-}(x_1 = L_1) = \mathbf{R_{12}}\vec{q}_1^{+}(x_1 = L_1) + \mathbf{T_{21}}\vec{q}_2^{-}(x_2 = 0). \tag{B1b}$$

Plugging in our expressions for $\vec{q}(\hat{x})$, we get

$$\begin{aligned} P_2^i v_{gx,2}^i u_2^i = {} & T_{12}^{ij}\left(P_1^j e^{-\gamma_1^j}v_{gx,1}^j u_1^j + \left\{\mathbf{\Phi}_{1,f}[\mathbf{A}_1^{-1}(\mathbf{F}_1^1\vec{P}_1 + \mathbf{F}_1^2\vec{B}_1)]\right\}^j\right) \\ & + R_{21}^{ij}\left(B_2^j e^{-\gamma_2^j}v_{gx,2}^j u_2^j + \left\{\mathbf{\Phi}_{2,b}[\mathbf{A}_2^{-1}(\mathbf{F}_2^1\vec{P}_2 + \mathbf{F}_2^2\vec{B}_2)]\right\}^j\right), \end{aligned} \tag{B2a}$$

$$\begin{aligned} B_2^i v_{gx,1}^i u_1^i = {} & R_{12}^{ij}\left(P_1^j e^{-\gamma_1^j}v_{gx,1}^j u_1^j + \left\{\mathbf{\Phi}_{1,f}[\mathbf{A}_1^{-1}(\mathbf{F}_1^1\vec{P}_1 + \mathbf{F}_1^2\vec{B}_1)]\right\}^j\right) \\ & + T_{21}^{ij}\left(B_2^j e^{-\gamma_2^j}v_{gx,2}^j u^j + \left\{\mathbf{\Phi}_{2,b}[\mathbf{A}_2^{-1}(\mathbf{F}_2^1\vec{P}_2 + \mathbf{F}_2^2\vec{B}_2)]\right\}^j\right), \end{aligned} \tag{B2b}$$

where the i, j superscripts indicate the phonon mode and u^i, u^j are the summation weights associated with phonon modes i and j, respectively. The sum over j is implied.

The matrices $\mathbf{\Phi}_f$ and $\mathbf{\Phi}_b$ are defined as

$$[\mathbf{\Phi}_f]^{\lambda,m} = \int_0^1 \frac{C_\lambda\cos(m\pi\hat{x}')}{Kn_\lambda}e^{-\gamma_\lambda(1-\hat{x}')}d\hat{x}' = \frac{M}{c}C_\lambda L[F^2]^{\lambda,m}, \tag{B3}$$

$$[\mathbf{\Phi}_b]^{\lambda,m} = \int_0^1 \frac{C_\lambda\cos(m\pi\hat{x}')}{Kn_\lambda}e^{-\gamma_\lambda\hat{x}'}d\hat{x}' = \frac{M}{c}C_\lambda L[F^1]^{\lambda,m}, \tag{B4}$$

with $M = 2\sum_\lambda C_\lambda/\tau_\lambda$ and $c = 1$ if $m = 0$ or $c = 2$ if $m \neq 0$.

Note that the bold variables are matrices. Multiplication between vectors is elemental multiplication. Figure 4 depicts how one can build the matrix equation from these boundary interface conditions.

2. Partially specular transmission

To account for both specular and diffuse reflection and transmission, the interface boundary conditions can be written as

$$\begin{aligned} & P_2^{i,s}v_{gx,2}^i u_2^i + P_2^{i,d}\sum_{\lambda\in\omega^i} v_{gx,2}^\lambda u_2^\lambda \\ & = T_{12}^{ij,s}\left(P_1^{j,s}e^{-\gamma_1^j}v_{gx,1}^j u_1^j + \left\{\mathbf{\Phi}_{1,f}^s[\mathbf{A}_1^{-1}(\mathbf{F}_1^{1,s}\vec{P}_1^s + \mathbf{F}_1^{2,s}\vec{B}_1^s)]\right\}^j\right) \\ & \quad + T_{12}^{ij,d}\left(P_1^{j,d}\sum_{\lambda\in\omega^j} e^{-\gamma_1^\lambda}v_{gx,1}^\lambda u_1^\lambda + \left\{\mathbf{\Phi}_{1,f}^d[\mathbf{A}_1^{-1}(\mathbf{F}_1^{1,d}P_1^d + \mathbf{F}_1^{2,d}\vec{B}_1^d)]\right\}^j\right) \\ & \quad + R_{21}^{ij,s}\left(B_2^{j,s}e^{-\gamma_2^j}v_{gx,2}^j u_2^j + \left\{\mathbf{\Phi}_{2,b}^d[\mathbf{A}_2^{-1}(\mathbf{F}_2^{1,s}\vec{P}_2^s + \mathbf{F}_2^{2,s}\vec{B}_2^s)]\right\}^j\right) \\ & \quad + R_{21}^{ij,d}\left(B_2^{j,d}\sum_{\lambda\in\omega^j} e^{-\gamma_2^\lambda}v_{gx,2}^\lambda u_2^\lambda + \left\{\mathbf{\Phi}_{2,b}^d[\mathbf{A}_2^{-1}(\mathbf{F}_2^{1,d}\vec{P}_2^d + \mathbf{F}_2^{2,d}\vec{B}_2^d)]\right\}^j\right), \end{aligned} \tag{B5}$$

where the superscripts s and d correspond to specular and diffuse scattering, respectively. The summations over $\lambda \in \omega^i$

$$P_2^i v_{gx,2}^i u_2^i = T_{12}^{ij}\left[P_1^j e^{-\gamma_1^j}v_{gx,1}^j u_1^j + \left[\mathbf{\Phi}_{1,f}\left[\mathbf{A}_1^{-1}\left(\mathbf{F}_1^1\vec{P}_1 + \mathbf{F}_1^2\vec{B}_1\right)\right]\right]^j\right]$$
$$+ R_{21}^{ij}\left[B_2^j e^{-\gamma_2^j}v_{gx,2}^j u_2^j + \left[\mathbf{\Phi}_{2,b}\left[\mathbf{A}_2^{-1}\left(\mathbf{F}_2^1\vec{P}_2 + \mathbf{F}_2^2\vec{B}_2\right)\right]\right]^j\right]$$

$$B_1^i v_{gx,1}^i u_2^i = R_{12}^{ij}\left[P_1^j e^{-\gamma_1^j}v_{gx,1}^j u_1^j + \left[\mathbf{\Phi}_{1,f}\left[\mathbf{A}_1^{-1}\left(\mathbf{F}_1^1\vec{P}_1 + \mathbf{F}_1^2\vec{B}_1\right)\right]\right]^j\right]$$
$$+ T_{21}^{ij}\left[B_2^j e^{-\gamma_2^j}v_{gx,2}^j u_2^j + \left[\mathbf{\Phi}_{2,b}\left[\mathbf{A}_2^{-1}\left(\mathbf{F}_2^1\vec{P}_2 + \mathbf{F}_2^2\vec{B}_2\right)\right]\right]^j\right]$$

$$\begin{bmatrix} A & B \\ C & D \end{bmatrix}\begin{bmatrix} B_1 \\ P_2 \end{bmatrix} = \begin{bmatrix} E & 0 \\ F & 0 \end{bmatrix}\begin{bmatrix} B_2 \\ P_3 \end{bmatrix} + \begin{bmatrix} 0 & G \\ 0 & H \end{bmatrix}\begin{bmatrix} B_0 \\ P_1 \end{bmatrix}$$

FIG. 4. Schematic indicating how Eq. (B2) can be written as a matrix equation.

Published under license by AIP Publishing.

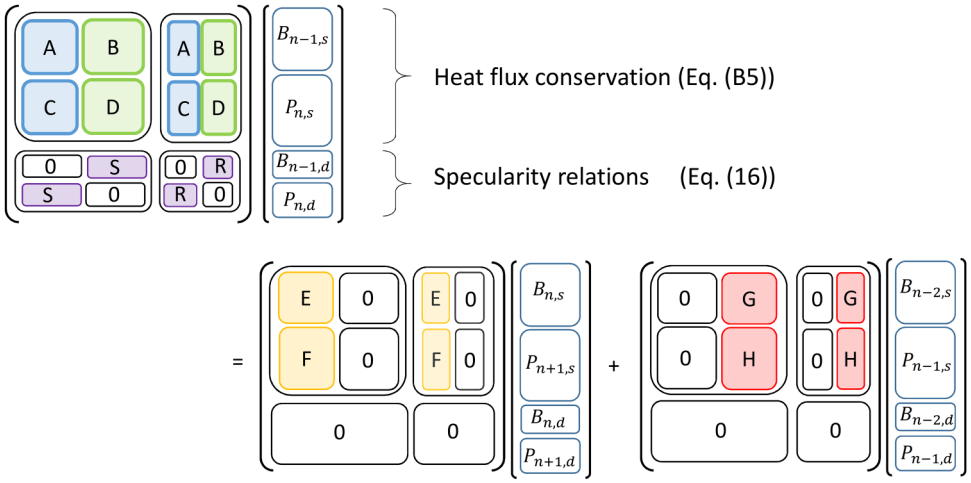

FIG. 5. Schematic indicating how matrices are modified to incorporate partial specularity. Constraints from boundary conditions of interface are given by Eq. (B5), and the constraints from the definition of specularity are given by Eq. (16). For the part of the matrix that defines partial specularity, *R* and *S* are the non-zero parts resulting from Eq. (16).

mean that the sum includes phonons of the same frequency as phonon i.

Recall that P^s and B^s contain N_λ elements, where N_λ is the number of phonon modes; P^d and B^d contain N_ω elements, where N_ω is the number of frequency bins. Then, $\mathbf{T}^s_{12}$ is a $N_{\lambda,2} \times N_{\lambda,1}$ matrix and $\mathbf{T}^d_{12}$ is a $N_{\lambda,2} \times N_{\omega,1}$ matrix. Similarly, $\mathbf{R}^s_{12}$ is a $N_{\lambda,1} \times N_{\lambda,1}$ matrix and $\mathbf{R}^d_{12}$ is a $N_{\lambda,1} \times N_{\omega,1}$ matrix. The diffuse reflection and transmission matrices have the same value for phonons of the same frequency—in essence, they are performing an averaging operation on the incident phonons.

A similar expression can be found for the B_1 coefficients that corresponds to the phonons propagating away from the interface. Figure 5 shows how including partial specularity changes the matrices in the matrix equation.

REFERENCES

[1]M. Zebarjadi, K. Esfarjani, M. S. Dresselhaus, Z. F. Ren, and G. Chen, Energy Environ. Sci. **5**, 5147 (2012).
[2]C. J. Vineis, A. Shakouri, A. Majumdar, and M. G. Kanatzidis, Adv. Mater. **22**, 3970 (2010).
[3]G. J. Snyder and E. S. Toberer, Nat. Mater. **7**, 105 (2008).
[4]D. G. Cahill, P. V. Braun, G. Chen, D. R. Clarke, S. Fan, K. E. Goodson, P. Keblinski, W. P. King, G. D. Mahan, A. Majumdar, H. J. Maris, S. R. Phillpot, E. Pop, and L. Shi, Appl. Phys. Rev. **1**, 011305 (2014).
[5]D. K. Ma, H. R. Ding, H. Meng, L. Feng, Y. Wu, J. Shiomi, and N. Yang, Phys. Rev. B **94**, 165434 (2016).
[6]L. Yang, N. Yang, and B. Li, Nano Lett. **14**, 1734 (2014).
[7]H. Honarvar, L. Yang, and M. I. Hussein, Appl. Phys. Lett. **108**, 263101 (2016).
[8]Y. Pennec, J. O. Vasseur, B. Djafari-Rouhani, L. Dobrzynski, and P. Deymier, Surf. Sci. Rep. **65**, 229 (2010).
[9]S. Yang, J. H. Page, Z. Liu, M. L. Cowan, C. T. Chan, and P. Sheng, Phys. Rev. Lett. **93**, 024301 (2004).
[10]A. A. Maznev, O. B. Wright, and M. O., New J. Phys. **13**, 013037 (2011).
[11]C. Colvard, R. Merlin, M. V. Klein, and A. C. Gossard, Phys. Rev. Lett. **45**, 298 (1980).
[12]V. Narayanamuri, H. Stormer, M. A. Chin, and A. C. Gossard, Phys. Rev. Lett. **43**, 2012 (1979).
[13]N. Zen, T. A. Puurtinen, T. J. Isotalo, S. Chaudhuri, and I. J. Maasilta, Nat. Commun. **5**, 3435 (2014).
[14]M. Maldovan, Nat. Mater. **14**, 667 (2015).
[15]S. M. Lee, D. G. Cahill, and R. Venkatasubramanian, Appl. Phys. Lett. **70**, 2957 (1997).
[16]J. Ravichandran, A. K. Yadav, R. Cheaito, P. B. Rossen, A. Soukiassian, S. Suresha, J. C. Duda, B. M. Foley, C.-H. Lee, Y. Zhu, A. W. Lichtenberger, J. E. Moore, D. A. Muller, D. G. Schlom, P. E. Hopkins, A. Majumdar, R. Ramesh, and M. A. Zurbuchen, Nat. Mater. **13**, 168 (2014).
[17]M. N. Luckyanova, J. Garg, K. Esfarjani, A. Jandl, M. T. Bulsara, A. J. Schmidt, A. J. Minnich, S. Chen, M. S. Dresselhaus, Z. Ren, E. A. Fitzgerald, and G. Chen, Science **16**, 936 (2012).
[18]J. Carrete, B. Vermeersch, L. Thumfart, R. R. Kakodkar, G. Trevisi, P. Frigeri, L. Seravalli, J. P. Feser, A. Rastelli, and N. Mingo, J. Phys. Chem. C **122**, 4054 (2018).
[19]R. Cheaito, C. A. Polanco, S. Addamane, J. Zhang, A. W. Ghosh, G. Balakrishnan, and P. E. Hopkins, Phys. Rev. B **97**, 085306 (2018).
[20]W. Ren, H. Li, L. Gao, Z. Zhang, C. Long, H. Ji, X. Niu, Y. Lin, and Z. Wang, Nano Res. **10**, 247 (2018).
[21]R. Venkatasubramanian, Phys. Rev. B **61**, 3091 (2000).
[22]B. Saha, Y. R. Koh, J. Comparan, S. Sadasivam, J. L. Schroeder, M. Garbrecht, A. Mohammed, J. Birch, T. Fisher, A. Shakouri, and T. D. Sands, Phys. Rev. B **93**, 045311 (2016).
[23]M. V. Simkin and G. D. Mahan, Phys. Rev. Lett. **84**, 927 (2000).
[24]G. Chen, J. Heat Transfer **121**, 945 (1999).
[25]B. Yang and G. Chen, Phys. Rev. B **67**, 195311 (2003).
[26]A. J. Minnich, J. Phys.: Condens. Matter **27**, 053202 (2015).
[27]D. Broido and T. Reinecke, Phys. Rev. B **70**, 081310 (2004).
[28]Y. Chen, D. Li, J. R. Lukes, Z. Ni, and M. Chen, Phys. Rev. B **72**, 174302 (2005).
[29]J. Garg and G. Chen, Phys. Rev. B **87**, 140302 (2013).
[30]J. Garg, N. Bonini, and N. Marzari, Nano Lett. **11**, 5135 (2011).
[31]Z. Tian, K. Esfarjani, and G. Chen, Phys. Rev. B **86**, 235304 (2012).

Published under license by AIP Publishing.

[32]R. Frieling, M. Radek, S. Eon, H. Bracht, and D. E. Wolf, Appl. Phys. Lett. **105**, 132104 (2014).
[33]B. Latour, S. Volz, and Y. Chalopin, Phys. Rev. B **105**, 014307 (2014).
[34]Y. Wang, H. Huang, and X. Ruan, Phys. Rev. B **90**, 165406 (2014).
[35]X.-K. Chen, Z.-X. Xie, W.-X. Zhou, L.-M. Tang, and K.-Q. Chen, Appl. Phys. Lett. **109**, 023101 (2016).
[36]A. Giri, P. E. Hopkins, J. G. Wessel, and J. C. Duda, J. Appl. Phys. **118**, 165303 (2015).
[37]A. France-Lanord, S. Merabia, T. Albaret, D. Lacroix, and K. Termentzidis, J. Phys.: Condens. Matter **26**, 355801 (2014).
[38]W. Zhang, T. S. Fisher, and N. Mingo, Numer. Heat Transfer B Fundam. **51**, 333 (2007).
[39]E. Landry and A. McGaughey, Phys. Rev. B **79**, 075316 (2009).
[40]G. Chen, Phys. Rev. B **57**, 14958 (1998).
[41]J.-P. M. Peraud and N. G. Hadjiconstantinou, Phys. Rev. B **93**, 045424 (2016).
[42]D. Abarbanel and J. Maaseen, J. Appl. Phys. **121**, 204305 (2017).
[43]J. Kaiser, T. Feng, J. Maassen, X. Wang, X. Ruan, and M. Lundstrom, J. Appl. Phys. **121**, 044302 (2017).
[44]C. Hua and A. J. Minnich, J. Appl. Phys. **117**, 175306 (2015).
[45]L. Lindsay, D. A. Broido, and T. Reinecke, Phys. Rev. B **20**, 165201 (2013).
[46]Q. Hao, G. Chen, and M. S. Jeng, J. Appl. Phys. **106**, 114321 (2009).
[47]J.-P. M. Peraud and N. G. Hajiconstantinous, Phys. Rev. B **91**, 235321 (2015).
[48]G. Chen, *Nanoscale Energy Transport and Conversion: A Parallel Treatment of Electrons, Molecules, Phonons, and Photons* (Oxford University Press, 2005).
[49]J. M. Ziman, *Electrons and Phonons: The Theory of Transport Phenomena in Solids* (Oxford University Press, 1960).
[50]Y. Zhang, D. Ma, Y. Zang, X. Wang, and N. Yang, Front. Energy Res. **6**, 00048 (2018).

Published under license by AIP Publishing.